Symmetry Breaking in Linearly Coupled Dynamical Lattices

G. Herring, P.G. Kevrekidis. B.A. Malomed, R. Carretero-González,
and D.J. Frantzeskakis

January 2, 2008

Publication Number: CSRCR2008-03

Computational Science & Engineering Faculty and Students Research Articles

Database Powered by the Computational Science Research Center Computing Group & Visualization Lab

COMPUTATIONAL SCIENCE & ENGINEERING

SAN DIEGO STATE UNIVERSITY

Computational Science Research Center
College of Sciences
5500 Campanile Drive
San Diego, CA 92182-1245
(619) 594-3430

Symmetry breaking in linearly coupled dynamical lattices

G. Herring* and P. G. Kevrekidis
Department of Mathematics and Statistics, University of Massachusetts, Amherst, Massachusetts 01003-4515, USA

B. A. Malomed
Department of Physical Electronics, Faculty of Engineering, Tel Aviv University, Tel Aviv 69978, Israel

R. Carretero-González
Nonlinear Dynamical Systems Group,† Department of Mathematics and Statistics, and Computational Science Research Center, San Diego State University, San Diego, California, 92182-7720, USA

D. J. Frantzeskakis
Department of Physics, University of Athens, Panepistimiopolis, Zografos, Athens 15784, Greece
(Received 19 April 2007; published 27 December 2007)

We examine one- and two-dimensional models of linearly coupled lattices of the discrete-nonlinear-Schrödinger type. Analyzing ground states of the system with equal powers (norms) in the two components, we find a symmetry-breaking phenomenon beyond a critical value of the total power. Asymmetric states, with unequal powers in their components, emerge through a subcritical pitchfork bifurcation, which, for very weakly coupled lattices, changes into a supercritical one. We identify the stability of various solution branches. Dynamical manifestations of the symmetry breaking are studied by simulating the evolution of the unstable branches. The results present the first example of spontaneous symmetry breaking in two-dimensional lattice solitons. This feature has no counterpart in the continuum limit because of the collapse instability in the latter case.

DOI: 10.1103/PhysRevE.76.066606 PACS number(s): 05.45.Yv

I. INTRODUCTION

Dynamical lattices and their applications have become an area of increasing interest over the past decade, as shown by a multitude of recent reviews of the topic [1–3]. This growth was driven by a wide array of physical realizations, in fields as diverse as light propagation in optical waveguide arrays [4], dynamics of Bose-Einstein condensates (BECs) in periodic potentials (optical lattices) [5], micromechanical cantilever arrays [3], models of DNA [6], and others. A key model that has been widely used in each of the above areas is the discrete nonlinear Schrödinger (DNLS) equation [2]. In these applications, it emerges either as a tight-binding approximation from the underlying continuum description (as in the case of BECs trapped in optical lattices), or via an envelope-wave expansion of the physical field (such as the electromagnetic wave in the optical systems).

One aspect of this class of discrete dynamical models that remains perhaps less explored concerns their multicomponent generalizations, which are relevant to many fields where dynamical lattices are natural models. For instance, in the application to waveguide arrays, one may consider settings with two orthogonal polarizations of light [7], or two different wavelengths [8]. Similarly, in the BEC context, one may consider multispecies condensates in the form of mixtures of different hyperfine states in ^{87}Rb [9,10] or ^{23}Na [11], and mixtures of different atomic species, such as Na-Rb, K-Rb, Cs-Rb, Li-Rb, and Li-Cs (see, e.g., Ref. [12], and references therein).

While the above settings are typically modeled by systems of DNLS equations, which are coupled by nonlinear terms, familiar examples being the cross-phase modulation in optics, or the terms accounting for collisions between atoms belonging to different BEC species, it is also relevant to consider *linearly coupled* DNLS equations (in other settings, these may be linearly coupled Ablowitz-Ladik equations [13]; a system of linearly coupled Toda lattices was also considered in Ref. [14]). In the context of optics, systems of linearly coupled DNLS equations are relevant to various applications: linear coupling may occur among two polarization modes inside each waveguide, being induced by a twist of the core (for linear polarizations), or by the birefringence (for circular polarizations). Linear coupling between two modes also takes place in arrays of dual-core waveguides [8]. On the other hand, in BECs, the linear coupling may be imposed by an external microwave or radio-frequency field, which can drive Rabi [15] or Josephson [16] oscillations between populations of two different states.

A notable effect induced by the linear coupling in nonlinear bimodal or dual-core systems is *spontaneous symmetry breaking* in two-component solitons. This effect was previously studied in continuum optical models with the cubic [17,18], quadratic [19], and cubic-quintic [20] nonlinearities, including the symmetry breaking of two-component *gap solitons* in dual-core fiber Bragg gratings [21,22]. Similar problems were recently explored in models of dual-core BEC-holding traps, including a planar two-channel configuration with the self-attractive BEC loaded into it [23], and a

*Present address: Cameron University, Department of Mathematical Sciences, Lawton, OK, 73505-6377.
†URL: http://nlds.sdsu.edu/

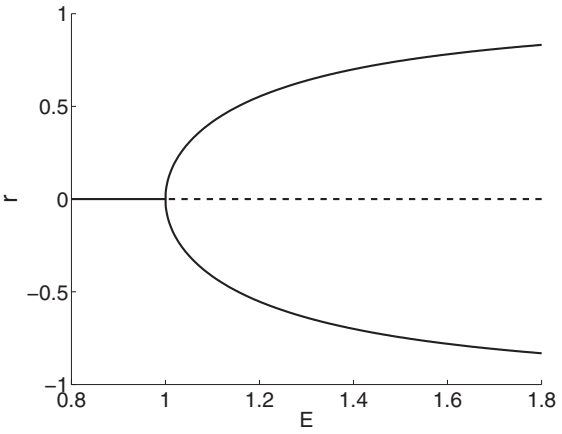

FIG. 1. The bifurcation diagram for the discrete solitons in the anticontinuum limit, $\epsilon=0$; r and E are the asymmetry parameter and the half of the total squared norm, respectively (definitions are given in the text). The solid and dashed lines show stable and unstable solutions, respectively.

system of two linearly coupled Gross-Pitaevskii equations with the self-repulsive nonlinearity and periodic (optical-lattice) potential in each of them. The latter model makes it possible to predict the symmetry breaking in two-component matter-wave solitons of the gap type [24]. As concerns discrete settings, the symmetry breaking of two-component solitons was found e.g., in linearly coupled Ablowitz-Ladik [13] lattices.

An important characteristic of the symmetry-breaking bifurcation is its *subcritical* (alias *backward*) or *supercritical* (alias *forward*) character, which is determined by the direction of the branches of asymmetric solutions emerging at the bifurcation point (examples of the supercritical and subcritical bifurcations are given in Figs. 1 and 2, respectively). In particular, the bifurcations found in the models of dual-core fibers with the cubic [17,18] and cubic-quintic nonlinearities [20] are subcritical, while in the model with the quadratic nonlinearities, as well as in models for gap solitons [21–24], they are supercritical (with some exceptions [22]).

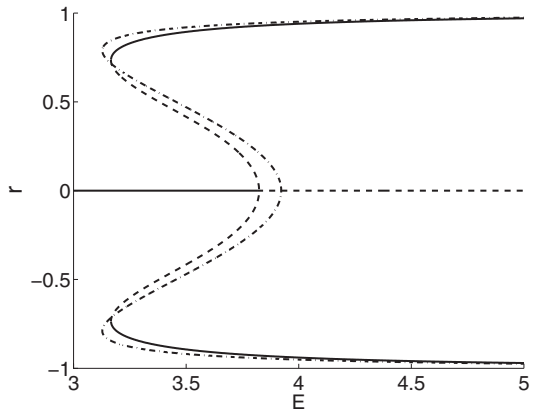

FIG. 2. The bifurcation diagrams for $\epsilon=1.6$ in the 1D model. The dashed-dotted line indicates solutions found by means of the variational approximation, while solid and dashed lines show, respectively, numerically found stable and unstable steady-state solutions.

Motivated by the above-mentioned results, in this work we aim to consider a system of two DNLS equations coupled (solely) by linear terms, and explore the symmetry-breaking bifurcation of two-component discrete solitons in it. In the optical setting, the system describes an array of twin-core optical waveguides, presenting a discrete counterpart of the well-known model of the nonlinear dual-core fiber [17,18]. A similar model was also proposed as a means for realization of all-optical switching in ultrashort photonic-crystal couplers [25]. In terms of BECs, the model applies to a mixture of two spin states, which undergo mutual linear interconversion under the action of a spin-flipping resonant electromagnetic wave (as mentioned above), assuming that the mixture is trapped in a deep optical lattice, and the Feshbach-resonance technique [26] is used to suppress the nonlinear interaction between the components.

In both media (optical and atomic), the basic model takes the following form:

$$iU_t = K\epsilon\Delta_2 U + KV + |U|^2 U,$$

$$iV_t = K\epsilon\Delta_2 V + KU + |V|^2 V, \tag{1}$$

where $U=U(\vec{x},t)$ and $V=V(\vec{x},t)$ are wave functions of the two species in BEC, or electric-field envelopes of the two coupled modes in optics ($\vec{x}$ is realized as a discrete vectorial coordinate), Δ_2 is the ordinary finite-difference Laplacian (see below), K is the strength of the linear coupling between fields U and V, and ϵ determines the couplings between adjacent sites of the lattice. For convenience, the full lattice-coupling constant is defined as $K\epsilon$ (this convention will allow us to eliminate K from the analysis presented below).

It may be relevant to mention that a counterpart of system (1) with *discrete time* may represent coupled map lattices (CMLs), which have been studied as models of spatiotemporal dynamics in various networks [27], including such effects as phase separation and nucleation in bistable systems [28], and synchronization of chaotic maps [29]. Discrete solitons and, accordingly, the symmetry breaking in related stationary states (if any) may be common to both the coupled DNLS equations and CMLs (although their stability properties may not be necessarily identical). Examining the dynamical effect of the considerations presented herein for CMLs may be an interesting question for future studies, in its own right.

Thus, our objective is to find and explore in detail the symmetry-breaking bifurcation of the ground-state single-pulse solution of Eqs. (1), similar to the earlier studies performed in continuum models in Refs. [17–20]. We will address this problem analytically—by means of a variational approximation (VA)—and numerically, via computations of the steady-state bifurcations and numerical analysis of the linear stability, as well as through direct simulations testing the stability or instability of the states under consideration. We will produce a complete bifurcation diagram of the discrete model. An advantage of performing this analysis in the discrete setting is that the bifurcation diagram can be obtained not only for one-dimensional (1D) lattices, but also for their two-dimensional (2D) counterparts. The latter is impossible in usual continuum models of the cubic-NLS type because of the collapse [30]. However, as demonstrated in

Ref. [31] (see also Ref. [2]), the DNLS with sufficiently weak intersite coupling [i.e., small coefficient ϵ in Eqs. (1)] gives rise to *stable* discrete 2D solitons. This permits us to construct a bifurcation diagram for the 2D lattice too, and compare it to the 1D counterpart. To the best of our knowledge, symmetry-breaking bifurcations have never been analyzed before in a 2D model with the cubic nonlinearity.

The paper is structured as follows. In Sec. II we present the model and analytical results, based on the variational method. In Sec. III, numerical results are reported. Finally, we summarize the findings and discuss directions for future work in Sec. IV.

II. MODEL AND ANALYTICAL CONSIDERATIONS

In what follows, we seek for steady-state solutions to system (1), in the usual form

$$V(\vec{x},t) = \sqrt{K}v(\vec{x})\exp[-iK(\mu - 2D\epsilon)t],$$

$$U(\vec{x},t) = \sqrt{K}u(\vec{x})\exp[-iK(\mu - 2D\epsilon)t], \tag{2}$$

where $u(\vec{x})$ and $v(\vec{x})$ are real-valued functions, μ is the chemical potential or propagation constant in the BEC/optical model, shifted by constant D, which is $D=1$ and 2 for the 1D and 2D lattice, respectively. Substituting these expressions in Eqs. (1) leads to stationary equations, which, in the 1D model, take the form

$$\mu u_n = \epsilon\bar{\Delta}_1 u_n + v_n + u_n^3,$$

$$\mu v_n = \epsilon\bar{\Delta}_1 v_n + u_n + v_n^3, \tag{3}$$

with $\bar{\Delta}_1 w_n \equiv w_{n+1} + w_{n-1}$. In the 2D case, the stationary equations are

$$\mu u_{n,m} = \epsilon\bar{\Delta}_2 u_{n,m} + v_{n,m} + u_{n,m}^3,$$

$$\mu v_{n,m} = \epsilon\bar{\Delta}_2 v_{n,m} + u_{n,m} + v_{n,m}^3, \tag{4}$$

where $\bar{\Delta}_2 w_{n,m} \equiv w_{n+1,m} + w_{n-1,m} + w_{n,m+1} + w_{n,m-1}$.

Below, we aim to construct symmetric ($u=v$) and asymmetric ($u \neq v$) solutions of Eqs. (3) and (4). In order to develop an analytical approximation to the solutions, we resort to the variational method [32]. To this end, we notice that Eqs. (3) and (4) can be derived from the following Lagrangians:

$$L_{1D} = \sum_{n=-\infty}^{\infty}\left[-\frac{\mu}{2}(u_n^2 + v_n^2) + \frac{1}{4}(u_n^4 + v_n^4) + u_n v_n \epsilon(u_{n+1}u_n + v_{n+1}v_n)\right], \tag{5}$$

$$L_{2D} = \sum_{m,n=-\infty}^{\infty}\left[-\frac{\mu}{2}(u_{n,m}^2 + v_{n,m}^2) + \frac{1}{4}(u_{n,m}^4 + v_{n,m}^4) + u_{n,m}^4 v_{n,m}^4 + \epsilon(u_{n+1,m}u_{n,m} + u_{n,m+1}u_{n,m} + v_{n+1,m}v_{n,m} + v_{n,m+1}v_{n,m})\right], \tag{6}$$

Further, we employ natural discrete-soliton *ansätze*, $\{u_n, v_n\} = \{A, B\}e^{-\lambda|n|}$ and $\{u_{n,m}, v_{n,m}\} = \{A, B\}e^{-\lambda|n|}e^{-\lambda|m|}$, with free constants A, B, and $\lambda > 0$, in the 1D and 2D cases, respectively. This choice is motivated both by the exponential decay of the solutions' tails far from the soliton's center and by the fact that only this type of trial function makes the approximation really tractable [33]. Note that, introducing different amplitudes A and B, we admit a possibility of *asymmetric solitons*, within the framework of the variational approximation.

Plugging the *ansätze* into Eqs. (5) and (6), and analytically evaluating the resulting geometric series, we arrive at the following expressions for the effective Lagrangians:

$$L_{1D} = \left[AB - \frac{\mu}{2}(A^2 + B^2)\right]\coth\lambda + \frac{1}{4}(A^4 + B^4)\coth(2\lambda) + \epsilon(A^2 + B^2)\operatorname{cosech}\lambda, \tag{7}$$

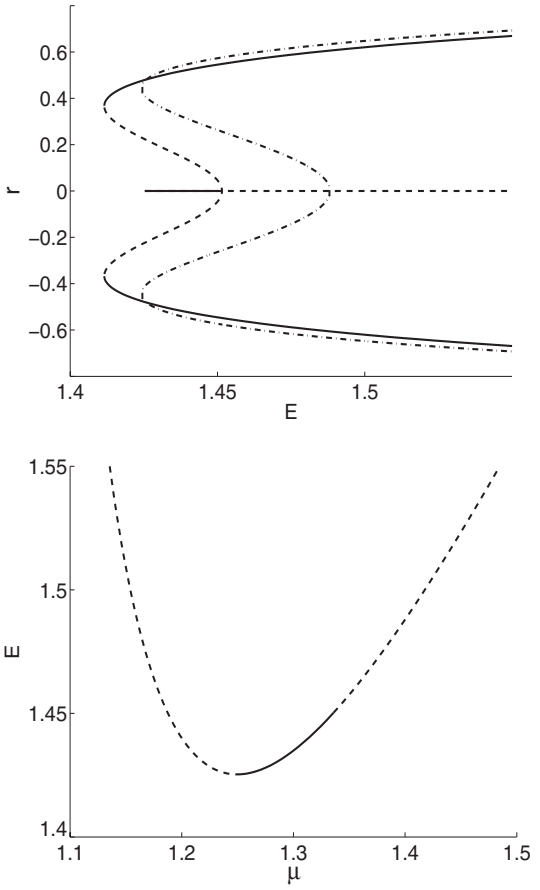

FIG. 3. The top panel shows the bifurcation diagram in the 2D model for $\epsilon=0.25$, in the same way (i.e., with the same meaning of the different curves) as the 1D diagram is shown in Fig. 2. The bottom panel displays the dependence of the solution's total squared norm E, upon the chemical potential μ, for the symmetric solutions. Unlike the 1D case, there are two different symmetric solutions for many values of E, resulting in both stable (solid line) and unstable (dashed lines) solutions for norms below the value at which the symmetric and asymmetric solution branches intersect.

$$L_{2D} = \left[AB - \frac{\mu}{2}(A^2 + B^2) \right] \coth^2 \lambda + \frac{1}{4}(A^4 + B^4)\coth^2 2\lambda + 2\epsilon(A^2 + B^2)(\mathrm{cosech}\,\lambda)\coth\lambda. \quad (8)$$

The static form of the Euler-Lagrange equations following from here, $\partial L_{1D,2D}/\partial(\lambda, A, B) = 0$, is

$$\frac{\mu}{2}(A^2 + B^2)\mathrm{cosech}^2\,\lambda - \frac{1}{2}(A^4 + B^4)\mathrm{cosech}^2\,2\lambda - AB\,\mathrm{cosech}^2\,\lambda - \epsilon(A^2 + B^2)\mathrm{cosech}\,\lambda\,\coth\lambda = 0,$$

$$-\mu A\coth\lambda + A^3\coth 2\lambda + B\coth\lambda + 2\epsilon A\,\mathrm{cosech}\,\lambda = 0,$$

$$-\mu B\coth\lambda + B^3\coth 2\lambda + A\coth\lambda + 2\epsilon B\,\mathrm{cosech}\,\lambda = 0,$$

for the 1D case, and

$$\mu(A^2 + B^2)\coth\lambda\,\mathrm{cosech}^2\,\lambda - (A^4 + B^4)\coth 2\lambda\,\mathrm{cosech}^2\,2\lambda - 2AB\coth\lambda\,\mathrm{cosech}^2\,\lambda - 2\epsilon(A^2 + B^2)(\mathrm{cosech}\,\lambda\coth^2\lambda + \mathrm{cosech}^3\,\lambda) = 0,$$

$$-\mu A\coth^2\lambda + A^3\coth^2 2\lambda + B\coth^2\lambda + 4\epsilon A\,\mathrm{cosech}\,\lambda\coth\lambda = 0,$$

$$-\mu B\coth^2\lambda + B^3\coth^2 2\lambda + A\coth^2\lambda + 4\epsilon B\,\mathrm{cosech}\,\lambda\coth\lambda = 0,$$

for the 2D soliton. Results obtained with numerically found solutions of these equations for A, B, and λ will be compared, in the next section, to full numerical solutions of Eqs. (3) and (4).

Another analytically tractable case corresponds to the anticontinuum limit, $\epsilon = 0$. For the symmetric branch, we then have $u_n = v_n = 0$ or $u_n = v_n = \sqrt{\mu - 1}$, while for the asymmetric branch, one needs to solve a system of algebraic equations, $\mu u_n = v_n + u_n^3$, $\mu + 1 = u_n^2 + u_n v_n + v_n^2$. The solution is shown in Fig. 1, which displays the symmetry-breaking bifurcation in the anticontinuum limit, by means of a plot of the *asymmetry measure*, $r \equiv (E_1 - E_2)/(E_1 + E_2)$, versus the average of the norms, $E = (E_1 + E_2)/2$, where $\{E_1, E_2\} = \Sigma_n\{u_n^2, v_n^2\}$ are the norms of the two components of the solution (in the BEC model, they are proportional to the number of atoms in the two atomic states, while in the optical setting they measure total powers of the beams in the two coupled lattices). As seen in the figure, the pitchfork bifurcation is *supercritical* in this limit (the latter feature will be compared to typical behavior for finite ϵ below).

III. NUMERICAL METHODS AND RESULTS

Numerical solutions to Eqs. (3) and (4) were found by dint of the method of the pseudoarclength (PAL) continuation (see [34,35] and the Appendix for more details).

Once the steady states were identified, their stability was examined in the framework of the linear stability analysis, by substituting the perturbed solution,

$$U(\vec{x}, t) = e^{-i\mu t}[u(\vec{x}) + a(\vec{x})e^{\lambda t} + b^*(\vec{x})e^{\lambda^* t}],$$

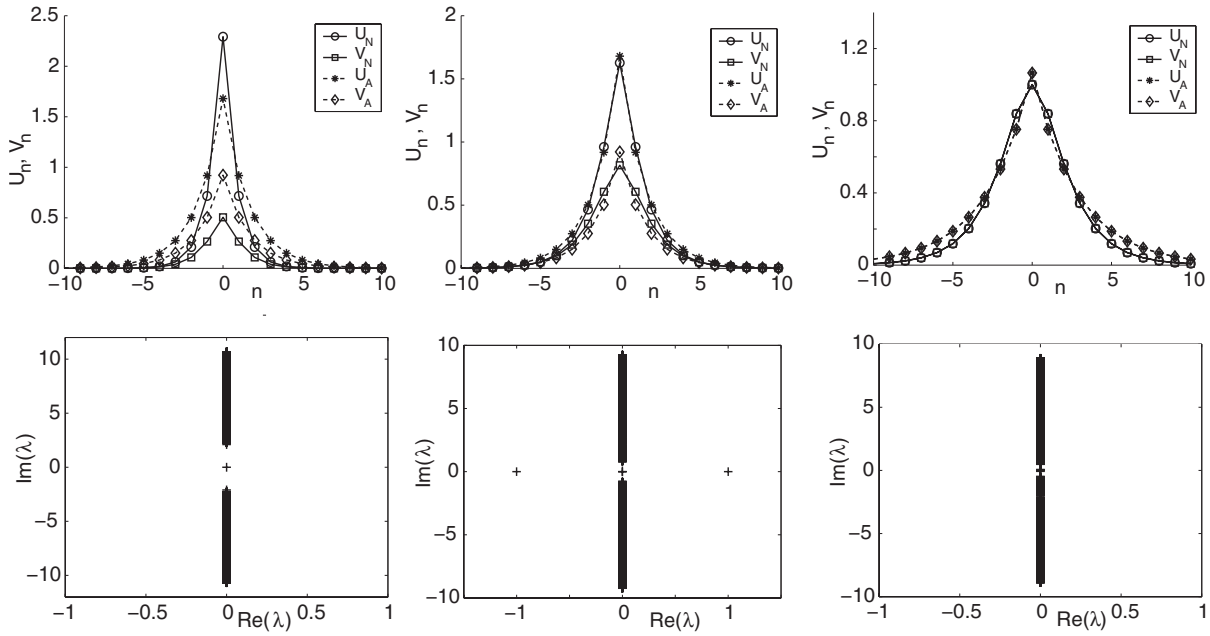

FIG. 4. Plots of solutions belonging to different branches in Fig. 2, at $E = 3.4$. The top-row figures show the solution profiles found by means of the numerical (U_N, V_N) and variational ("analytical", U_A, V_A) methods. The bottom-row plots illustrate the stability eigenvalues for the numerical solution. The first column presents a stable stationary asymmetric solution belonging to the outer (upper) branch in Fig. 2, the second column is an unstable asymmetric solution from the inner branch, and the last column is taken from the stable part of the family of symmetric solutions, with $r = 0$.

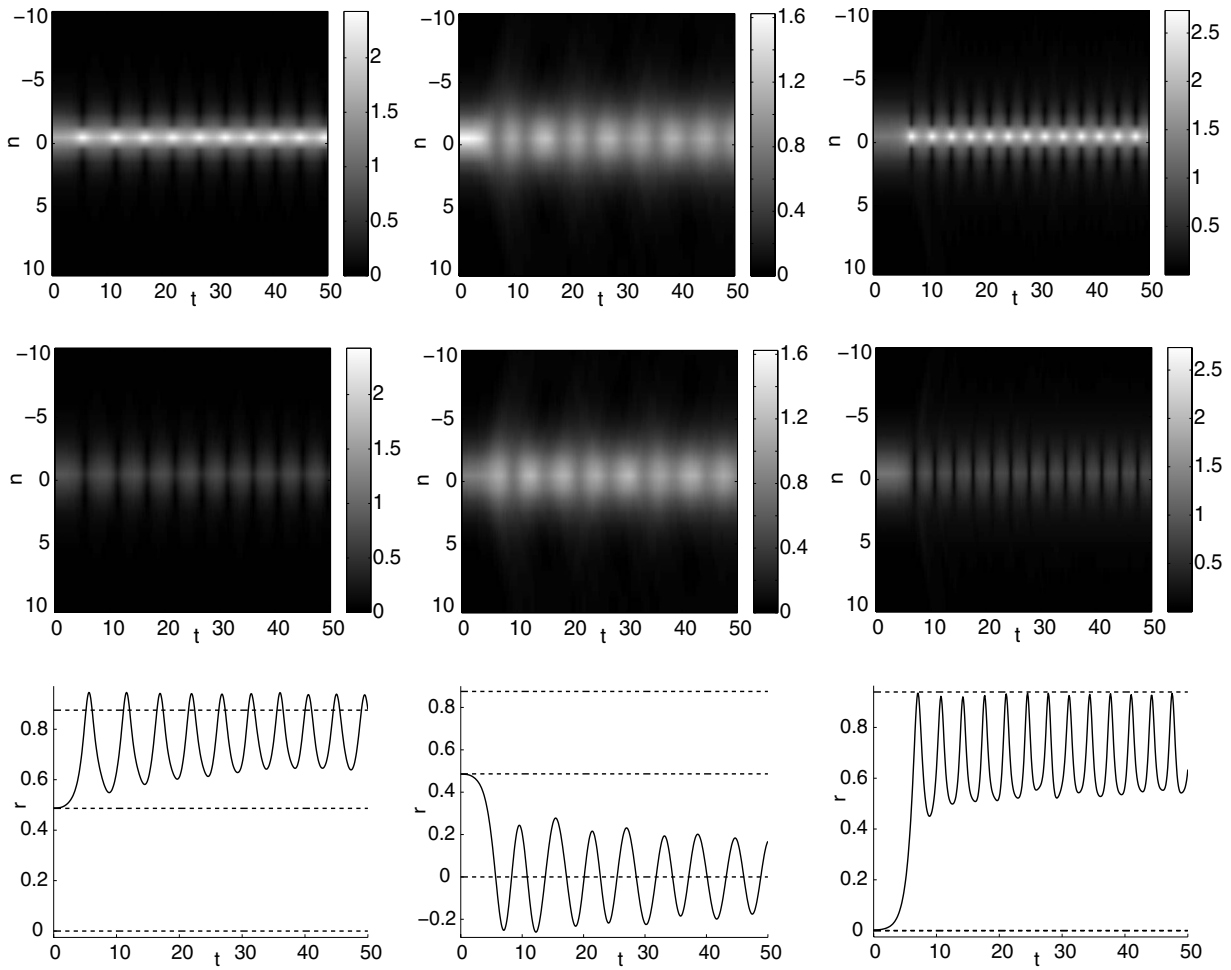

FIG. 5. Time-evolution plots for perturbed one-dimensional solutions from Fig. 2. The top (middle) row depicts the evolution of $|U|^2$ ($|V|^2$) by means of space-time contour plots. The first two columns pertain to two different perturbations of the solution shown in the second column of Fig. 4: the first column is generated by a perturbation which pushes the solution toward the upper stable asymmetric solution branch in the bifurcation diagram, while, in the second column, the initial perturbation pushes the solution toward the $r=0$ solution. The last column pertains to a perturbation of the unstable symmetric solution (belonging to the branch with $r=0$) at $E=4.1$, which pushes the solution toward the upper stable branch. The bottom row displays the value of asymmetry parameter r as the solutions evolve in time (solid line), and the constant value of r for the steady states at the same value of the norm (dashed horizontal lines).

$$V(\vec{x},t) = e^{-i\mu t}[v(\vec{x}) + c(\vec{x})e^{\lambda t} + d^*(\vec{x})e^{\lambda^* t}], \tag{9}$$

in Eqs. (1), with the asterisk standing for the complex conjugate. The linearized equations for perturbation eigenmodes a,b,c,d in expressions (9) were solved numerically, yielding the eigenvalues λ associated with them.

The results are summarized in Figs. 2 and 3, for the 1D and 2D cases, respectively. In the 1D case, the symmetric branch, with $r=0$, is stable for $E<3.82$. Beyond this critical point, it becomes unstable through a *subcritical* pitchfork bifurcation, due to its collision with two unstable asymmetric branches. The VA predicts this critical point at $E\approx 3.92$, in good agreement with the numerical findings. Further, at another critical value, $E=3.166$ (the corresponding VA prediction is $E\approx 3.128$), the unstable asymmetric branches turn back as stable ones, through a saddle-node bifurcation. Between the two critical points, both the symmetric branch and the outer asymmetric one are stable, hence there exists a region of bistability.

To additionally demonstrate the accuracy of the VA, Fig. 4 presents comparisons of the solution profiles at $E=3.4$, together with the spectral plane, $(\mathrm{Re}(\lambda),\mathrm{Im}(\lambda))$, for the corresponding eigenvalues, $\lambda \equiv \mathrm{Re}(\lambda) + i\,\mathrm{Im}(\lambda)$. Recall that, in Hamiltonian systems, such as the one considered here, if λ is an eigenvalue, so are also $-\lambda$, λ^*, and $-\lambda^*$, hence, if any eigenvalue with a nonzero real part exists, then the system is linearly unstable.

For those 1D solutions that are linearly unstable due to a real eigenvalue, such as the unstable asymmetric solutions for $3.166<E<3.82$, and the symmetric ones for $E>3.82$, we have examined their evolution in direct simulations of Eqs. (1), as shown in Fig. 5. For asymmetric unstable solutions, the outcome depends upon the nature of the initial perturbation, due to the presence of the bistability in the corresponding parameter range: the solution ends up oscillating around either the stable asymmetric solution, or the stable symmetric one. The evolution of the unstable symmetric branch naturally results in oscillations around the stable

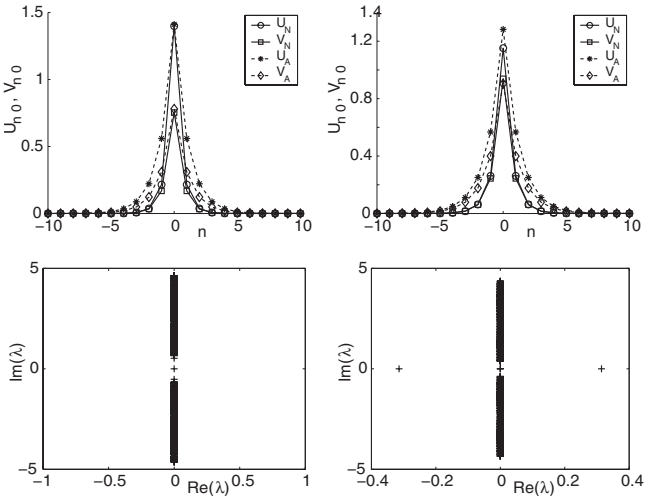

FIG. 6. Cross-section plots of the asymmetric solutions belonging to different branches in Fig. 3, at $E=1.435$. The top-row figures show the solutions found by means of the numerical (U_N, V_N) and variational ("analytical", U_A, V_A) methods, and the bottom-row plots display stability eigenvalues for the numerical solution. As can be seen, the first and second columns represent, respectively, stable and unstable solutions belonging to the upper (outer) and inner curves (asymmetric branches) of the bifurcation diagram, respectively.

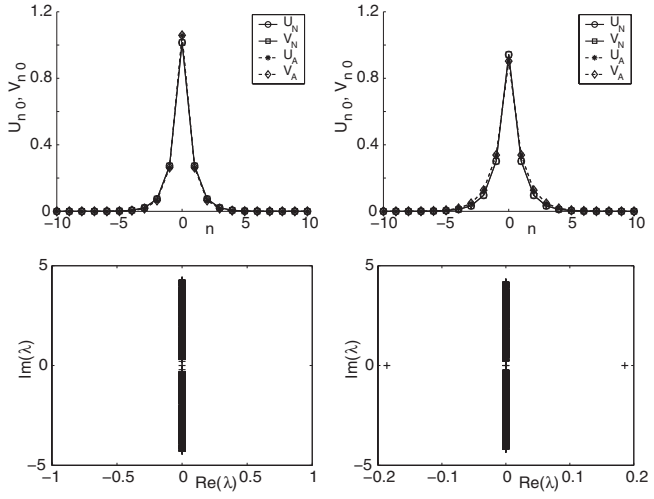

FIG. 7. Same as Fig. 6 for two symmetric solutions found at $E=1.435$.

asymmetric profile, which represents the ground state in that case.

A conclusion following from the comparison of Figs. 1 and 2 is that the bifurcation found in the anticontinuum limit (see Fig. 1) is definitely supercritical, unlike the weakly subcritical one in Fig. 2. This indicates that the character of the pitchfork bifurcation changes from subcritical to supercritical with the increase of discreteness, i.e., the decrease of ϵ. In particular, this transition should eliminate the unstable asymmetric branches. In accordance with this expectation, we have found that the unstable asymmetric solutions exist only for $\epsilon > 0.35$, in the 1D case.

We now turn to results for the 2D model, which are collected in Fig. 3. These results are even more interesting, for a number of reasons. On the one hand (as mentioned above) the bifurcation diagram has no counterpart in usual 2D continuum models, as the 2D solutions are always subject to collapse, in the continuum. In single-component models, the discreteness is well known to arrest the collapse [31,36], generating branches of localized solutions that may be stable at sufficiently small values of the intersite coupling constant (at a given chemical potential), or at sufficiently large values of the chemical potential (at a given intersite coupling) [31]. Furthermore, in the 2D case, for a given value of the norm, there are two coexisting symmetric solutions, one (taller and narrower) with a larger chemical potential, which is stable, and one (shorter and wider) with a smaller chemical potential, which is unstable. As Fig. 3 implies, the symmetry-breaking weakly subcritical pitchfork bifurcation *typically* occurs on the stable branch of the symmetric solution, the corresponding critical point in Fig. 3 being $E \approx 1.45$. Similar to the 1D case, there also exists a saddle-node bifurcation between the unstable and stable asymmetric branches, which occurs at $E \approx 1.411$ and is responsible for the turning point.

In the 2D model too, the VA correctly approximates the qualitative behavior of the numerical results, even though the less accurate nature of the 2D ansatz prevents a quantitative matching of the resulting bifurcation diagrams. Actual profiles of the numerical solutions and their VA-predicted counterparts are shown in Figs. 6 and 7, for the asymmetric and symmetric branches, respectively, at $E=1.435$. Two additional remarks are in order here. First, similar to the 1D case, the 2D bifurcation changes its character from weakly subcritical (as observed in Fig. 3) to supercritical (as seen in the anticontinuum limit of $\epsilon=0$) at $\epsilon \approx 0.19$. On the other hand, as ϵ further increases, the stable portion of the symmetric branch (in Fig. 3) shrinks and eventually disappears at $\epsilon > 0.29$.

Finally, we have again examined the dynamics of linearly unstable solutions, with appropriate perturbations, through direct simulations, as shown in Figs. 8 and 9. In the former figure, we have explored how the bistability, which is shown for a range of E in Fig. 3, "kicks" the unstable asymmetric solution either in the direction of its stable asymmetric counterpart, or toward the stable symmetric solution (it is relevant to stress here, in connection with Fig. 3, that, while the symmetric solution has a norm threshold at $E \approx 1.425$, the stable asymmetric solution can, in principle, be found at *lower* norms than the symmetric one, thus allowing the system to effectively decrease its "excitation threshold" [37]). In the latter figure, we consider the unstable symmetric branch, both when a stable symmetric branch does not exist, in which case the solution becomes asymmetric (top row), and when a stable symmetric branch does exist, in which case the system evolves toward that solution (bottom row).

IV. CONCLUSIONS

In this work, we have introduced the model based on two linearly coupled lattices with the cubic nonlinearity, and investigated its dynamical properties in detail. We have demonstrated that, in a number of respects, the discrete system

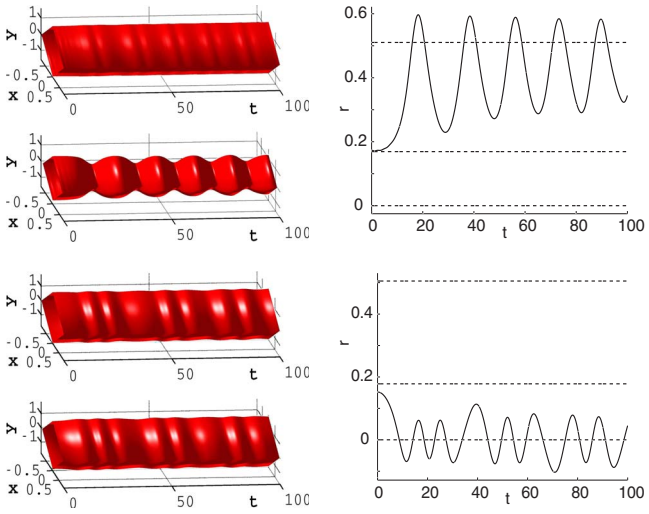

FIG. 8. (Color online) Time-evolution plots for a perturbed unstable solution in Fig. 6. The top-row perturbation pushes the solution toward the upper stable part of the curve, while the bottom-row perturbation pushes it to the symmetric branch. The left column shows the three-dimensional space-time evolution of isodensity contours of the U (respective top subpanels) and V (respective bottom subpanels) modes, while the right column shows the evolution of the asymmetry measure r, from an unstable steady state to a stable one (both are denoted by dashed lines).

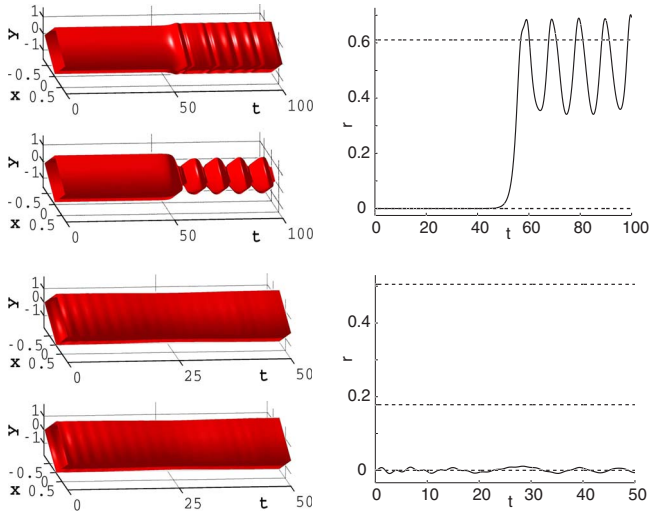

FIG. 9. (Color online) Similar to the previous figure: the time-evolution plots for two perturbed unstable symmetric states. The top row pertains to the solution with $E=1.5$, and the bottom row is for the solution from Fig. 7. In the top row, the perturbation pushes the solution toward the upper asymmetric branch, while in bottom row the perturbation initiates the evolution of the solution toward the stable symmetric state.

emulates its continuum 1D counterpart with the same (cubic) nonlinearity, analyzed earlier in Refs. [17,18,24]. On the other hand, the lattice model gives rise to different features. Even in the 1D setting, varying the strength of the lattice intersite coupling may be used to switch the character of the pitchfork bifurcation from subcritical to supercritical, as the coupling gets weaker (in the anticontinuum limit the bifurcation is definitely supercritical). In the most interesting 2D setting, no example of the bifurcation diagram has ever been reported before, to the best of our knowledge, since, in the continuum limit, the symmetry-breaking models with the self-focusing nonlinearity are irrelevant because of the inherent collapse. Furthermore, the discreteness induces the presence of both stable and unstable branches of symmetric solutions, thus enriching the bifurcation diagram. In the 2D case, not only is it possible for weaker lattice coupling to turn the bifurcation from subcritical to supercritical, but it is also possible for the lattice (when the bifurcation is subcritical) to possess a *lower existence threshold* for asymmetric states than for symmetric ones. All of these features demonstrate critical modifications that the discreteness imposes on the well-known symmetry-breaking picture in continuum models.

The effects analyzed in this work are amenable to experimental observation in arrays of twin-core nonlinear optical waveguides, and in two-component BEC trapped in the deep optical lattice. In particular, in the latter setting, the spontaneous symmetry breaking implies the transition of the condensate into a state with imbalanced total spin. Such states may be easily probed in the experiment by applying an external dc spatially uniform magnetic field parallel to the spins. In particular, a weak field may easily deform the ideal pitchfork bifurcation into its asymmetric variant, which may be an interesting effect by itself. In terms of the dual-core optical waveguide arrays, physical manifestations of the spontaneous symmetry breaking may be quite interesting too, as the collective character of the effect can make it essentially stronger than in an individual double-core waveguide, where its observation has never been reported.

It might be quite interesting to examine similar features in 3D models, and compare the results with their 2D and 1D counterparts. Of perhaps even more physical interest, especially in terms of the linearly coupled hyperfine states in BECs, would be to add nonlinear interaction between the two components. It would be particularly interesting to examine how the symmetry-breaking phenomenology is affected by the gradual increase of the nonlinear-coupling coefficient (scattering length of interspecies atomic collisions, in terms of BEC). This study is currently in progress and the results will be reported elsewhere.

Note added in proof. In a very recent work by Gubeskys and Malomed [38], the symmetry breaking in a two-dimensional setting was considered in a continuum model of two parallel pancake-shaped Bose-Einstein condensates (BECs), under the action of the potential of a square optical lattice. The model is based on a system of two Gross-Pitaevskii equations with linear coupling between them.

APPENDIX: PSEUDOARCLENGTH CONTINUATION

The focus of the class of techniques known as numerical continuation is the calculation of solutions over a large range of parameter values. These techniques are designed to solve a system of parametrized equations

$$G(u,\lambda)=0, \tag{A1}$$

where $(u,\lambda)\in\mathbb{R}^N\times\mathbb{R}$.

The easiest and most frequently utilized numerical continuation technique is parameter continuation. This technique takes a previously determined solution u_0, found for some parameter value λ_0, and uses it as an initial guess in an iterative method (here we have used Newton's method) to determine the solution for a nearby parameter value $\lambda_1=\lambda_0+\Delta\lambda$. This process then repeats for each newly found solution.

The weakness of the parameter continuation method is its inability to handle points where $G_u(u,\lambda)$ is singular, typically resulting in the failure of Newton's method, and a number of other iterative methods, to converge. As a result, other numerical continuation techniques have been produced to tackle these problems. The technique we chose to use here was pseudoarclength continuation [34].

Pseudoarclength continuation is the same as parameter continuation, in that they both use a previously calculated solution (u_0,λ_0) to determine a nearby solution. However, pseudoarclength continuation addresses the singularity problem by introducing a pseudoarclength parameter s into the system (A1) via the inclusion of an additional equation $F(u,\lambda,s)=0$, which must be chosen such that $F(u_0,\lambda_0,0)=0$. Many different functions have been suggested for F and for this project

$$F(u,\lambda,s) = \|u-u_0\|^2 + |\lambda-\lambda_0|^2 - s^2 \tag{A2}$$

was chosen. Basically, this function searches for solutions on the solution branch which are located at a Euclidean distance s from the known solution (u_0,λ_0). Based upon a function similar to that in Eq. (A2), the corresponding Jacobian

$$J(u,\lambda,s) = \begin{bmatrix} G_u(u,\lambda) & G_\lambda(u,\lambda) \\ F_u(u,\lambda,s) & F_\lambda(u,\lambda,s) \end{bmatrix} \tag{A3}$$

was shown to always be nonsingular in [35].

Having dealt with the problem of the nonsingular Jacobian, implementing the pseudoarclength method is simply a matter of expanding the iterative method used to find the initial solution to now solve the augmented system

$$G(u,\lambda) = 0,$$

$$F(u,\lambda,s) = 0. \tag{A4}$$

In the case of Newton's method, the iterations become

$$\begin{bmatrix} u^{k+1} \\ \lambda^{k+1} \end{bmatrix} = \begin{bmatrix} u^k \\ \lambda^k \end{bmatrix} - J^{-1}(u^k,\lambda^k,s) \begin{bmatrix} G(u^k,\lambda^k) \\ F(u^k,\lambda^k,s) \end{bmatrix}, \tag{A5}$$

where the function F is changed after every new solution is found to now use the newly found solution in place of u_0 and λ_0 in Eq. (A2).

[1] S. Aubry, Physica D **103**, 201 (1997); S. Flach and C. R. Willis, Phys. Rep. **295**, 181 (1998); D. Hennig and G. Tsironis, *ibid.* **307**, 333 (1999).

[2] P. G. Kevrekidis, K. Ø. Rasmussen, and A. R. Bishop, Int. J. Mod. Phys. B **15**, 2833 (2001).

[3] M. Sato, B. E. Hubbard, and A. J. Sievers, Rev. Mod. Phys. **78**, 137 (2006).

[4] D. N. Christodoulides, F. Lederer, and Y. Silberberg, Nature (London) **424**, 817 (2003); Yu. S. Kivshar and G. P. Agrawal, *Optical Solitons: From Fibers to Photonic Crystals* (Academic Press, San Diego, 2003).

[5] V. A. Brazhnyi and V. V. Konotop, Mod. Phys. Lett. B **18**, 627 (2004); O. Morsch and M. Oberthaler, Rev. Mod. Phys. **78**, 179 (2006); P. G. Kevrekidis and D. J. Frantzeskakis, Mod. Phys. Lett. B **18**, 173 (2004).

[6] M. Peyrard, Nonlinearity **17**, R1 (2004).

[7] J. Meier, J. Hudock, D. Christodoulides, G. Stegeman, Y. Silberberg, R. Morandotti, and J. S. Aitchison, Phys. Rev. Lett. **91**, 143907 (2003).

[8] J. Hudock, P. G. Kevrekidis, B. A. Malomed, and D. N. Christodoulides, Phys. Rev. E **67**, 056618 (2003).

[9] C. J. Myatt, E. A. Burt, R. W. Ghrist, E. A. Cornell, and C. E. Wieman, Phys. Rev. Lett. **78**, 586 (1997).

[10] D. S. Hall, M. R. Matthews, J. R. Ensher, C. E. Wieman, and E. A. Cornell, Phys. Rev. Lett. **81**, 1539 (1998).

[11] D. M. Stamper-Kurn, M. R. Andrews, A. P. Chikkatur, S. Inouye, H.-J. Miesner, J. Stenger, and W. Ketterle, Phys. Rev. Lett. **80**, 2027 (1998).

[12] P. G. Kevrekidis, H. Susanto, R. Carretero-González, B. A. Malomed, and D. J. Frantzeskakis, Phys. Rev. E **72**, 066604 (2005).

[13] B. A. Malomed and J. Yang, Phys. Lett. A **302**, 163 (2002).

[14] P. G. Kevrekidis and B. A. Malomed, Phys. Lett. A **303**, 328 (2002).

[15] R. J. Ballagh, K. Burnett, and T. F. Scott, Phys. Rev. Lett. **78**, 1607 (1997); B. Deconinck, P. G. Kevrekidis, H. E. Nistazakis, and D. J. Frantzeskakis, Phys. Rev. A **70**, 063605 (2004).

[16] P. Ohberg and S. Stenholm, Phys. Rev. A **59**, 3890 (1999); J. Williams, R. Walser, J. Cooper, E. Cornell, and M. Holland, *ibid.* **59**, R31 (1999).

[17] N. Akhmediev and J. M. Soto-Crespo, Phys. Rev. E **49**, 4519 (1994).

[18] P. L. Chu, B. A. Malomed, and G. D. Peng, J. Opt. Soc. Am. B **10**, 1379 (1993);; B. A. Malomed, I. M. Skinner, P. L. Chu, and G. D. Peng, Phys. Rev. E **53**, 4084 (1996).

[19] W. C. K. Mak, B. A. Malomed, and P. L. Chu, Phys. Rev. E **55**, 6134 (1997); **57**, 1092 (1998)

[20] L. Albuch and B. A. Malomed, Math. Comput. Simul. **74**, 312 (2007).

[21] W. C. K. Mak, B. A. Malomed, and P. L. Chu, J. Opt. Soc. Am. B **15**, 1685 (1998).

[22] Y. J. Tsofe and B. A. Malomed, Phys. Rev. E **75**, 056603 (2007); Proc. SPIE **6604**, 660419 (2007).

[23] M. Matuszewski, B. A. Malomed, and M. Trippenbach, Phys. Rev. A **75**, 063621 (2007).

[24] A. Gubeskys and B. A. Malomed, Phys. Rev. A **75**, 063602

(2007).
[25] A. Locatelli, D. Modotto, D. Paloschi, and C. De Angelis, Opt. Commun. **237**, 97 (2004).
[26] S. Inouye, M. R. Andrews, J. Stenger, H.-J. Miesner, D. M. Stamper-Kurn, and W. Ketterle, Nature (London) **392**, 151 (1998); J. Stenger, S. Inouye, M. R. Andrews, H.-J. Miesner, D. M. Stamper-Kurn, and W. Ketterle, Phys. Rev. Lett. **82**, 2422 (1999); J. L. Roberts, N. R. Claussen, J. P. Burke, Jr., C. H. Greene, E. A. Cornell, and C. E. Wieman, *ibid.* **81**, 5109 (1998); S. L. Cornish, N. R. Claussen, J. L. Roberts, E. A. Cornell, and C. E. Wieman, *ibid.* **85**, 1795 (2000); E. A. Donley, N. R. Claussen, S. L. Cornish, J. L. Roberts, E. A. Cornell, and C. E. Wieman, Nature (London) **412**, 295 (2001).
[27] K. Kaneko, Chaos **2**, 279 (1992), and other papers in this focus issue.
[28] G.-L. Oppo and R. Kapral, Phys. Rev. A **36**, 5820 (1987).
[29] F. S. de San Roman, S. Boccaletti, D. Maza, and H. Mancini, Phys. Rev. Lett. **81**, 3639 (1998).
[30] C. Sulem and P. L. Sulem, *The Nonlinear Schrödinger Equation* (Springer-Verlag, New York, 1999).
[31] P. G. Kevrekidis, K. Ø. Rasmussen, and A. R. Bishop, Phys. Rev. E **61**, 2006 (2000).
[32] B. A. Malomed, in *Progress in Optics*, edited by E. Wolf (North-Holland, Amsterdam, 2002), Vol. 43, p. 71.
[33] B. A. Malomed and M. I. Weinstein, Phys. Lett. A **220**, 91 (1996).
[34] E. L. Allgower and K. Georg, "Numerical Path Following," in *Handbook of Numerical Analysis*, edited by P. G. Ciarlet and J. L. Lions (North-Holland, Amsterdam, 1997), Vol. 5, pp. 3–207.
[35] H. B. Keller, "Numerical Solution of Bifurcation and Nonlinear Eigenvalue Problems," in *Applications of Bifurcation Theory*, edited by P. H. Rabinowitz (Academic Press, New York, 1977), pp. 359–384.
[36] G. Fibich and B. Ilan, Appl. Numer. Math. **44**, 63 (2003); N. Tzirakis and P. G. Kevrekidis, Math. Comput. Simul. **69**, 553 (2005).
[37] S. Flach, K. Kladko, and R. S. MacKay, Phys. Rev. Lett. **78**, 1207 (1997); M. Weinstein, Nonlinearity **12**, 673 (1999).
[38] A. Gubeskys and B. A. Malomed, Phys. Rev. A **76**, 043623 (2007).